Conservation of Modernism Movement Concrete: Tackling the Compatibility Issue of Retrofit Solutions with the Degraded Substrate

Travasso Jocelyn, Loic Gatti, and Tsangouri Eleni[(✉)]

Department of Mechanics of Materials and Constructions (MeMC), Vrije Universiteit Brussel (VUB), Pleinlaan 2, 1050 Brussels, Belgium
eleni.tsangouri@vub.be

Abstract. The conservation of Modernism heritage is of utmost importance today since the concrete heritage of the 20th century is now aged and faces severe durability issues. However, due to restrictions introduced considering their architectural identity and aesthetics, the repair and conservation interventions should be performed only if the reversibility of actions is ensured. The design of repair patches and retrofit layers should be based on this principle and at the same time performed in long-term and often in aggressive environments, indicatively sea exposure. This work report on recent experimental tests evaluating the compatibility criteria that should be established in order to ensure durability and the optimal mechanical performance of cement-based fiber-reinforced repair patches for degraded concrete. The adhesion to the degraded substrate is of utmost importance since bonding should lead to efficient interaction among materials, however should not alter the substrate consistency and response to service loads. The deterioration mechanism of chloride-ions exposure leading to concrete carbonation and rebars corrosion is tested by evaluating large open cracks as formed after bending of small-scale concrete slabs. The retrofit layering is applied after the accelerated exposure of the slabs to the chloride environment and evaluated by cyclic bending tests that follow. The compatibility of the materials under flexural stresses is monitored using an integrated inspection methodology: acoustic emission and digital image correlation, whereas the adhesion of the retrofit to the substrate is inspected using microscopy scanning and ultrasound pulse velocity. It is demonstrated that premature interfacial debonding can be linked to the incompatibility of materials due to different stiffness and lack of interlocking. This phenomenon can be catastrophic for future rehabilitation projects.

Keywords: Modernism concrete · chloride exposure · cracking · petrofit · restoration · premature failure

1 Introduction

1.1 Modernism Concrete: Exposure to Aggressive Chloride Environment

Exposed reinforced concrete is the material that embodies the Modern Movement in the second half of the 20th century and today shows pathological manifestations affecting both the functionality and safety of the constructions [1]. Recent case studies demonstrate the vulnerability of exposed concrete facades, naturally porous and irregular and inherently cracked [2], especially when exposed to a sea environment where accelerated reinforcement corrosion may call for early repair interventions [3]. With a future perspective on the climate change era, the rehabilitation of corroded Modernist concrete is of utmost importance since recent studies report that by 2100, a rise of up to 15% of the chloride concentrations on reinforced concrete exposed to sea environment [4] is expected, while the rising sea level will induce up to 18% lifetime reduction for marine concrete (the study focused in the climatic conditions in France [5]).

Engineers of today are challenged with the conservation of very recently valorized Modern concrete monuments (ie. World Heritage List of 1,050 properties; among them only 15 of contemporary architecture [6]) facing aggressive weathering. However, currently, inadequate guidelines exist for a rehabilitation methodology, and limited standardization is reported on the technical details of a restoration intervention. Indicatively, the debate between the casting of new external protection layering against the creation of replicas of dismantled segments (that ensure the architectural identity and aesthetic details of the original [6]) is open and introduces technical and philosophical questions [7].

1.2 Retrofit Interventions

Distress and deterioration of corroded concrete are expressed drastically by macro-cracking that leads to cover delamination [8], which may lead to significant flexural strength drop and accelerated shear failure [9]. The rehabilitation should be designed considering the material compatibility with the existing damaged concrete; therefore, o repair cement patches are often added as an extra chloride ingress barrier in the extended cover zone. However, the insight view of the underlying causes, the crack and delamination kinetics and the retrofit-original composite action is disregarded, leading to opposite effects: the premature collapse of the repair solution and accelerated deterioration of the structure [10]. A review of the recent bibliography demonstrated that limited information is available on the long-term performance of widespread technical solutions, especially in aggressive sea environments, such as ferrocement repair layering [11] or the addition of textiles on the retrofitting grout [12].

1.3 Research Objectives

This preliminary work aims to explore the potential of reinforced cement retrofit to control the cracks on modern concrete exposed to salt environments. For the first time in literature, large structural elements are loaded to trigger multiple cracks, while the fracture progress is monitored using advanced optical, microscopy and digital image

correlation (DIC) and acoustic, acoustic emission (AE) and ultrasound pulse velocity (UPV), inspection techniques. The data collected are critically analyzed to pinpoint the efficacy of the repair intervention and reveal the damage mechanisms that may lead to premature retrofit failure. The effect of surface morphology and salt depositions on the retrofit performance is also assessed. As a research outcome, a novel integrated inspection methodology is proposed, whereas the most important test variables that define materials compatibility will be identified, providing a guide for future interventions on the Modernism heritage.

2 Materials and Methods

In total, 15 concrete slabs are cast and tested in this test campaign. Normal concrete is cast and reinforced by the minimum steel reinforcement to ensure multiple cracking under four-point bending. The concrete slabs are designed to ensure optimal handling in the lab with geometry limited due to weight (no more than 20 kg, so that they can be comfortably carried around). Up to date, there is no standard in the bibliography for the slab design and the tests that trigger cracking, but also for the curing to aggressive environments. Three reference slabs are tested without being exposed to the sea environment. At least 9 slabs are immersed in salt water; among them 3 are retrofitted with AR glass textile-reinforced cement, while other 3 are retrofitted with ferrocement.

2.1 Concrete Casting

The concrete composition is given in Table 1. The dry components are mixed for 2 min before adding water. After 4 min of mixing, the concrete is poured into wooden molds, where 4 Φ8 ribbed steel rebars are mounted before casting (at the height of 20 mm from the bottom line). The molds have inner dimensions of 445 $\times$ 300 $\times$ 55 mm, and after casting, vibration is applied to the concrete for an additional minute. The concrete slab is sealed with plastic film and stored in ambient conditions (20 °C; $\pm$ 65% RH) for 48 h. Afterwards, the slabs are demolded and immersed in water (20 °C) for 28 days. Before testing, the slabs are removed from the water and dried for up to 3 days in ambient conditions.

Table 1. Concrete composition with the quantities presented per concrete slab.

Component	Content
Sand 0/2 mm	5.43 kg
Cement CEM I 32.5 N	2.43 kg
Small aggregates 2/8 mm	3.96 kg
Large aggregates 8/16 mm	6.40 kg
Water	1.2 lt

2.2 Four-Point Bending Cyclic Testing

The concrete slabs are loaded under four-point bending in quasi-static mode. The Instron 5885 universal testing bench is used and a load cell with 100 kN capacity is mounted. The loading frame is displacement controlled with a rate of 0.1 mm/min. The bending span at the bottom is fixed at 405 mm and the two loading pins stand at a distance of 200 mm.

A cracking cycle is performed initially to trigger damage on the slabs before the chloride exposure (Fig. 1a). During testing, multiple cracks form across the bending span and widen under extensive loading. With respect to the serviceability limit state for concrete, the loading ends as soon as the majority of cracks open wider than 0.5 mm. Unloading follows with a displacement rate of 1 mm/min leading to a final crack opening lower than 0.3 mm. The testing time, the applied load and the frame displacement are recorded by the Instron software, whereas the crack control is obtained by DIC (Fig. 2a).

The four-point bending test is repeated after curing in chloride environment and casting a retrofit layer, following the same testing procedure as at the cracks-triggering cycle (Fig. 1a).

2.3 Chloride Ingress

In an attempt to simulate the sea chloride environment, the concrete slabs were immersed in fresh water carrying 5 wt.% NaCl for 90 days after cracking. The samples are conditioned at 20 °C into plastic containers, sealed on top with a plastic film to avoid water evaporation. Every month, the slabs are removed from the water for 24 h, dried and tested by AE using the Hsu-Nielsen protocol (see Sect. 2.5).

2.4 Retrofit Casting

A 10 mm-thick cement layer is cast at the bottom of the concrete slabs with the aid of a wooden mold. The cement mix proportions (per weight) are 1:2:0.5 for the cement:sand:water respectively, whereas 20 mg of superplasticizer is added per layer to ensure optimal rheology and penetration through the textile layers. Two reinforcement textiles are considered: the metal wire mesh (ferrocement) and the alkali-resistant AR-glass (SITgrid 200). Two textile layers are cast: first, a 3 mm-thick layer of cement mortar is poured on top of the slab, then a layer of textile is added, followed by a 2 mm-thick mortar layer, ended with an extra layer of textile and a final 3 mm-thick mortar cover. After the retrofit casting, the slabs are sealed with a plastic film for 48 h, and then underwater curing is followed for up to 28 days before the re-loading cycle.

2.5 Inspection Methodology

An integrated inspection and monitoring methodology is implemented to thoroughly investigate the damage onset and progress on concrete slabs and quantify and track potential mechanical performance recovery after retrofitting. Optical microscopy and UPV are applied before and after each bending cycle, whereas AE Hsu-Nielsen tests are

performed in an intact and cracked state, and during the conditioning in a chloride environment. During bending tests, the DIC and AE provide insight into the crack formation and propagation (Fig. 2b).

Optical Microscopy. The concrete surface morphology and crack voids are inspected after exposure to the chloride environment using a portable Dino-Lite digital microscope with a resolution of 1.3 MP. Both macroscopic and closer view of the salt depositions are reported in this work.
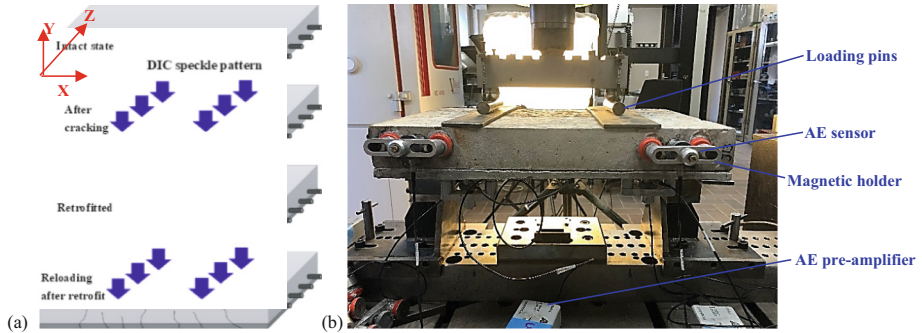

Fig. 1. a) Load-deflection curve projected with the opening of each crack (blue series) developed on one of the concrete slabs during the cracking cycle; b) The cracks formation and propagation stages are marked A-D and illustrated with the respective DIC strain maps.

Ultrasound Pulse Velocity (UPV). The wave velocity, directly linked to the material stiffness and presence of open cracks, is calculated in transmission mode using the Controls pulse generator devise that emits a 2500 V signal with a sampling rate of 2 MHz. The emitter is placed at the bottom zone of the slab side, whereas the receiver stands at the bottom of the other side (wave propagation distance 445 mm, see Fig. 3a). This way, an overall analysis of the cracked area is obtained at different testing moments: this study focuses on the ultrasound pulse velocity measured at the cracking stage and after the conditioning with chloride exposure. For comparison reasons, an additional UPV measurement is obtained at the bottom of the slab after the adhesion of the retrofit layer (same emitter/receiver distance).

Acoustic Emission and Pencil Lead Breaking Test. Acoustic Emission is applied throughout cyclic bending tests; how-ever, this analysis is out of the scope of this paper. In this work, the Hsu-Nielsen test performed before and after bending will be analyzed [13]. A pencil lead is broken in the vicinity of Sensor 1 (as illustrated in Fig. 3a), and the signal received by Sensor 4 is recorded. The amplitude changes after cracking and salt exposure will be analyzed herein to extract information on the attenuation rise induced by open cracks. It should be noted that after retrofit layering, the AE sensors are placed in the same position as before. The AE set-up details are summarized in Table 2.

Table 2. Acoustic Emission and Digital Image Correlation set-up details.

AE set-up		DIC set-up	
Pre-amplification	40 dB	Lenses focal length	17 mm
Amplitude threshold	35 dB	CCD camera resolution	2560 × 2058 pixels
Sensor type	R15 (150 kHz resonance)	Subset/Step/Strain window	21/7 pixels
Sampling rate	1 MSPS	Area of interest	440 × 65 mm
Frequency spectrum	10 kHz–2 MHz	Capturing rate	Each 3 s

Digital Image Correlation. A pair of high-resolution cameras are fixed facing the concrete slab side, as illustrated in Fig. 1a. Stereo-calibration is performed before testing to ensure that a 3D view of deformation and strain phenomena can be captured with the set-up details reported in Table 2. The Exx and Exy strain maps are selected in this work to pinpoint the presence of cracks and potential interfacial debonding. In Fig. 1a, the coordinate system is set for the DIC analysis.

3   Results

3.1   Test Design and Triggering of Chloride Exposure

In Fig. 2a, the load-deflection curve of a representative slab is presented as recorded at the first bending cycle. In parallel, the crack opening of each individual crack forming is tracked by DIC as illustrated on the Exx strain maps in Fig. 2b. With the use of the Vic3D point tracking tool, the crack opening at the slab's bottom line is extracted and plotted versus the load. The results compile to prove that four damage stages are developing: the early uncracked phase characterized by the concrete's flexural stiffness, ending as the first crack forms (point A); at the second stage, multiple cracks form at the bending zone reaching the knee-point B after which the load rises with a lower rate and plastic deformation begins. Eventually, all cracks get wider at the steel yielding stage, reaching point C marked due to a significant load drop. At that point, the cracks open unstably with high rates and it was decided that the loading ends at point D since all cracks have reached the compression zone and are wider than 0.5 mm. It should be noted that DIC tracks only the slab's side view, therefore cannot characterize damage evolving along the slab's width. As shown in Fig. 3a and for a representative slab, the cracks develop several inter-connected branches along the slab's width, indicating the complexity of cracks' interaction under bending loads and during the conditioning in aggressive environments.

Conditioning in a chloride environment follows and scanning with microscopy highlights the salt deposition at the concrete surface and into the cracks, as illustrated in Fig. 3b. The closer view of the crystal masses proves that the concrete is aggressively attacked by salt; therefore, the surface morphology and roughness have been severely modified after the conditioning. The filling of the open cracks by the salt can also be

catastrophic since further exposure to water and coverage with the retrofit layer may trigger salt particles expansion and local spalling, the latter being a mechanism that induces macroscopic interfacial debonding of the retrofit from the damaged concrete.
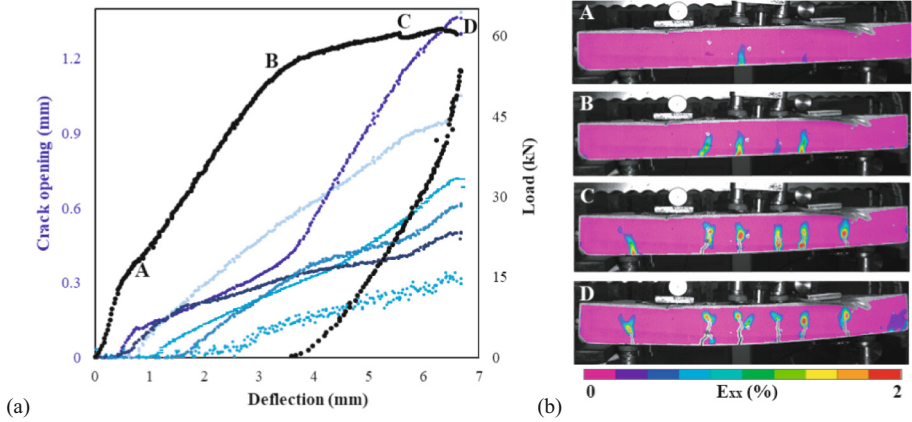

(a)   (b)

Fig. 2. a) Load-deflection curve projected with the opening of each crack (blue series) developed on one of the concrete slabs during the cracking cycle; b) The cracks formation and propagation stages are marked A-D and illustrated with the respective DIC strain maps.
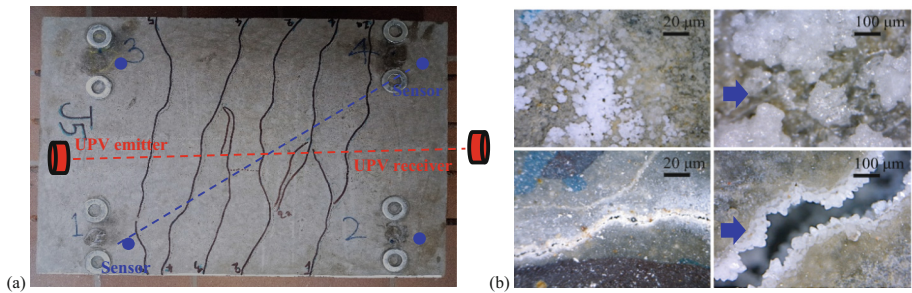

(a)   (b)

Fig. 3. a) Bottom view of the concrete slab with the inter-connected cracks marked in black color; b) Microscopic inspection of salt depositions at the concrete surface and through the crack.

3.2 Mechanical Performance After Retrofit

Due to space limitations, the reloading test will not be extensively reported in this paper; however, the UPV tracked before and after retrofit will briefly demonstrate the effectiveness of the repair method for concrete exposed to an aggressive chloride environment. In Fig. 4a, the UPV tracked throughout the length of the slabs is reported for two testing series: reference slabs (no exposure) and slabs treated in salt water for 3 months (Chloride exposure series). Remarkably, the UPV drops significantly after the conditioning compared to the reference series. This result that proves the detrimental effect of chloride

exposure on the material stiffness and may indicate further weakening at the open cracks attacked by salt. After retrofitting, the UPV drops for the reference series, an indication that UPV accuracy drops in the presence of concrete-retrofit and retrofit-textile interphase and due to the retrofit cement lower stiffness compared to concrete. Taking this into account, it is still remarkable that the retrofit intervention leads to UPV rise for the chloride-treated slabs. In other words, the retrofit covers the cracks, potentially fills the voids locally, and enhances the continuity among materials. The UPV recovery proves the beneficial role of retrofitting even in severely damaged concrete exposed to the sea environment. Similar trends are reported based on the AE pencil lead breaks analysis in Fig. 4b. The AR-glass textile reinforced cement retrofit managed an important amplitude recovery compared to the series of ferrocement retrofit. The difference reported herein requires further investigation concerning the adhesion among materials for both series.
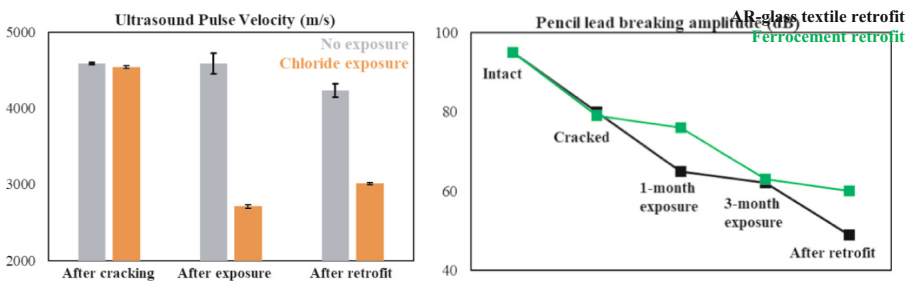

Fig. 4. a) Ultrasound pulse velocity at different testing stages as measured through the width of the slabs colored in grey for the non-exposed slabs and in orange for the slabs exposed to chloride environment; b) The amplitude of the signal as received by AE sensor and triggered by pencil lead breaking from a sensor standing at the other side of the bending span.

3.3   Interfacial Debonding Phenomena

The retrofit contribution to the slab's resistance to further service loads is tracked with the re-loading cycle. During this test, an important observation is reached based on DIC strain analysis summarized in Fig. 5. Two slabs are discussed and selected considering the E_{xy} strain distribution at the concrete-retrofit interphase as measured at the final loading stage (all cracks formed; steel yielding is present). One may notice that the slab presented in the right column of Fig. 5b develops significantly E_{xy} strain concentrated at the materials interface, a phenomenon attributed to premature debonding. No remarkable strain is evident for the other slab during testing, proving this way that effective concrete-retrofit bonding is reached; therefore, the retrofit layer follows the deflection of the slab under four-point bending. Remarkably, the cracks pattern is modified as interfacial debonding evolves, as illustrated with the E_{xx} strain maps in Fig. 5a. When comparing the strain distribution around the cracks before and after retrofitting, it is concluded that cracks form on the retrofit at the same locations as the pre-existing cracks. On the other hand, for the debonded series, due to interfacial debonding, the new cracks forming at the retrofit are not linked with the pre-existing cracks. There is a shift in cracks location,

proving that the retrofit does not restrain the pre-existing cracks, and additional cracking of the retrofit may lead to an early failure.
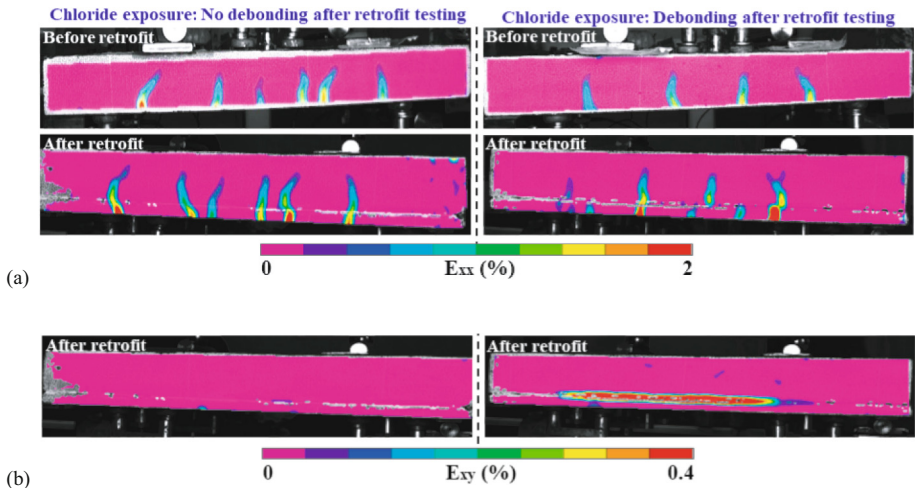

Fig. 5. a) DIC Exx strain maps for chloride-exposed slabs: with and without debonding phenomena; b) respective Exy strains.

It should be noted that the interfacial debonding was more evident for the ferrocement retrofit series, potentially due to the limited flexibility of the metal mesh. The latter observation is in agreement with the AE findings reported in Fig. 4b; therefore, the extensive attenuation can be attributed to limited materials adhesion. In the next step of this work, the retrofit is also exposed to chloride ingress in order to measure the corrosion effect on the metal mesh and the potential alkali-silica reaction on the AR-glass fibers. The ongoing research will be communicated extended in an upcoming journal publication.

4 Conclusions

The test campaign presented in this paper aims to simulate the exposure of Modernism concrete structures to aggressive chloride environments in an attempt to track damage and explore the potential of AR-glass textile/metal mesh reinforced cement retrofit. The detrimental effect of salt deposition on the concrete surface is well reported in the literature; however, the cracks filling by salt on large-scale concrete slabs is a topic that has not been extensively investigated at a macro-level (up to now, research focuses on micro-inspection and elemental analyses). Therefore, this work aims to communicate a breakthrough testing methodology considering bulk steel reinforced concrete slabs inspected with optical and acoustic non-destructive techniques. It is shown that the damaged concrete is extensively deteriorated after salt water exposure, a result that demonstrates the importance of crack kinetics for salt transportation. In the second phase,

the retrofit efficacy is in question for severely cracked concrete at which the surface is salt-saturated. This is due to premature interfacial debonding at the concrete-retrofit interface that may lead to a catastrophic collapse of the repair layer and unstable steel yielding. The research is ongoing, exploring further the retrofit resistance to chloride ingress and documenting the crack dynamics under continuous exposure to chloride environments.

References

1. Macdonald, S., Gonçalves, A.P.A.: Concrete conservation: outstanding challenges and potential ways forward. Int. J. Build. Pathol. Adapt. **38**(4), 607–618 (2020)
2. Araujo, A.D., Oliveira, C.D.A., Simão, T.R.D.S.: Current condition of the exposed concrete façades reinforcement of the Vilanova Artigas building: modern architectural heritage. Revista IBRACON de Estruturas e Materiais **14** (2020)
3. Ford, M., Gaudette, P., Slaton, D.: Restoring serenity: conservation of Minoru Yamasaki's North Shore Congregation Israel. J. Archit. Conserv. **27**(1–2), 104–116 (2021)
4. Sousa, M.L., Dimova, S., Athanasopoulou, A., Dyngeland, T., Pinto, A.: Expected Implications of Climate Change on the Corrosion of Structures. Publications Office of the European Union (2020)
5. Bastidas-Arteaga, E.: Reliability of reinforced concrete structures subjected to corrosion-fatigue and climate change. Int. J. Concrete Struct. Mater. **12**(1), 1–13 (2018). https://doi.org/10.1186/s40069-018-0235-x
6. Kahrovichandžic, L.: A Case Study: Restoration of Historical Museum in Sarajevo (1963)–A Modernist Ruin. Heritage Architecture Studies (2018)
7. MacDonald, S.: Authenticity is more than skin deep: Conserving Britain's postwar concrete architecture. Docomomo J. (1997)
8. Harrer, A., Gaudette, P.: Challenges of preserving modernist concrete. In: MATEC Web of Conferences, vol. 289, p. 07003. EDP Sciences (2019)
9. Zaki, A., Chai, H.K., Benhnia, A., Aggelis, D.G., Tan, J.Y., Ibrahim, Z.: Monitoring fracture of steel corroded reinforced concrete members under flexure by acoustic emission. Constr. Build. Mater. **136**, 609–618 (2017)
10. Charciarek, M., Derkowski, W.: A voice on Polish socialist brutalist architecture: protection of concrete element surfaces in the context of sustainable development. Wiadomości Konserwatorskie (2021)
11. Beßling, M., Groh, M., Koch, V., Auras, M., Orlowsky, J. Middendorf, B.: Repair and protection of existing steel-reinforced concrete structures with high-strength, textile-reinforced mortars. Buildings **12**(10) (2022)
12. Balamuralikrishnan, R., Al Madhani, M., Al Madhani, R.: Study on Retrofitting of RC Columns using Ferrocement full and strip wrapping, Civ. Eng. J. **5**(11) (2015)
13. Hsu, N.: Characterization and calibration of acoustic emission sensors. Mater. Eval. **39**, 60–68 (1981)